ChemPubSoc Europe

DOI: 10.1002/ejic.201501422

EurJIC European Journal of Inorganic Chemistry

Full Paper

Immobilized Catalysts

Ionic Immobilization of Silicotungstic Acid on Amine-Functionalized Zirconia: A Mesoporous Catalyst for Esterification of Maleic Acid

Meenakshi Ramalingam,[a] Sundar Manickam,[a] Kutti Rani Srinivasalu,*[a] Mohammed Bilal Ismail,[a] and Easwaramoorthy Deivanayagam[a]

Abstract: Silicotungstic acid ($H_4SiW_{12}O_{40}$) has been immobilized onto the mesopores of amine-functionalized zirconia by exploitation of electrostatic interactions. The ionic grafting of silicotungstic acid was confirmed by XPS, FTIR, UV/Vis-DRS and TGA analysis. The mesoporosity of the material was confirmed through N_2 adsorption/desorption analysis. The morphology of the material was established by TEM analysis. The immobilized silicotungstate material was found to be an efficient heterogeneous catalyst for selective esterification of maleic acid with butan-1-ol. A 98 % level of conversion of maleic acid and 82 % selectivity for dibutyl maleate within 5 h at 95 °C was achieved. The catalyst could be reused thrice without loss of activity.

Introduction

Polyoxometallates (POMs)/heteropolyacids are nanodimensional anionic clusters based on oxygen and different transition-metal ions such as V, Nb, Mo and W, with metal-oxygen octahedrons as the basic structural units.[1] Polyoxometallates are highly acidic with multiple-electron redox properties and have hence attracted much attention as acid and oxidation catalysts for various reactions.[2–4] Although polyoxometallates are used as efficient catalysts in various organic reactions, the low surface areas (1–10 $m^2\ g^{-1}$) and high solubilities of POMs in polar solvents often result in poor catalyst/product separation. This problem can be overcome by heterogenizing the POMs with appropriate supports, which increases the specific surface area of the catalyst and hence enhances the catalytic activity.[5] The heterogenization of polyoxometallates and its applications in the production of catalysts has been explored extensively.[6–15]

Mesoporous materials such as MCM-41, SBA-15 and zirconia, with high surface areas, uniform and controllable pore sizes, and well-ordered packing of pores, have been used as supports for polyoxometallates.[13,16,17] Impregnation is the simplest and most convenient method for immobilizing soluble POMs within the solid supports. The major drawbacks of this method are uneven distribution of POMs and their leaching during catalytic reactions.[18,19] A more appropriate method would be to functionalize the support with a silane and then to immobilize POMs by covalent[20] or noncovalent interactions.[21] This functionalization imparts enhanced stability to the immobilized catalytic species.[22]

Zirconia has been used as an excellent catalyst support for POMs because ZrO_2 nanoparticles offer several advantages such as chemical inertness, high melting point and excellent thermal stability even under harsh reducing or oxidizing conditions.[23,24] Zirconia-supported polyoxometallates have been investigated as catalysts for various chemical transformations such as oxidation of alkenes[25,26] and esterification.[27] The functionalization of zirconia with different groups has been widely reported.[28–33] In particular, the structural basicity of mesoporous zirconia (m-ZrO_2)T functionalized with amine groups resulted in excellent yields of Knoevenegal condensation products at room temperature under solvent-free conditions, as reported by Parida et al.[32] Similarly, Cu-anchored amine-functionalized m-ZrO_2 was an efficient, reusable catalyst for aryl–sulfur coupling for the synthesis of value-added diarylsulfides.[33]

The immobilization of polyoxometallates on amine-functionalized zirconia by exploitation of electrostatic interactions had not previously been reported. The free-amine-functionalized zirconia should be protonated by the acidic heteropolyacid (e.g., $H_4SiW_{12}O_{40}$) protons to form (propyl $NH_3^+)_4$ $[SiW_{12}O_{40}]^{4-}$. Furthermore, the oxygen atoms of silicotungstic acid should enter into weak hydrogen bonding with free hydroxy groups of the zirconia network, thereby increasing the fixation of Keggin units firmly within the pores. This synergetic effect of strong electrostatic interactions and weak hydrogen bonding may decrease the leaching of $[SiW_{12}O_{40}]^{4-}$ in high-temperature liquid-phase reactions: esterification, for example.

Esters are important intermediates in the synthesis of fine chemicals, plasticisers, food preservatives, pharmaceuticals etc.[18,34,35] Esters are generally produced in industry by use of mineral acid catalysts such as hydrofluoric acid, sulfuric acid

[a] Department of Chemistry, B.S. Abdur Rahman University, Seethakathi Estate, Vandalur, Chennai, Tamil Nadu 600048, India
E-mail: skrani@bsauniv.ac.in
http://www.bsauniv.ac.in/mode/faculty/action/details/name/225-Dr.-S.-KUTTI-RANI

Supporting information for this article is available on the WWW under http://dx.doi.org/10.1002/ejic.201501422.

etc., which are corrosive and have to be neutralized after the reaction for disposal.[35,36] The use of ecologically friendly heterogeneous solid acid catalysts would be a better alternative for esterification reactions.[19,27,35,37] Silicotungstic acid (15 wt.-%) supported on hydrous zirconia has been used as an efficient and stable solid acid catalyst for the esterification of various acids with alcohols with 100 % selectivity.[27] The liquid-phase esterification of acetic acid with butanol in the presence of phosphotungstic acid supported on ZrO_2, SiO_2 and carbon was reported by Sepúlveda et al.[19] Hβ zeolite was found to be more active than Al-MCM-41 molecular sieves in the esterification of maleic anhydride with methanol.[35] Esterification of maleic anhydride with ethanol over Al-MCM-41 (Si/Al-50, 100) and Hβ zeolite resulted in a 95 % yield of diethyl maleate at the end of the ninth hour.[37]

In this work we aimed at low loading of silicotungstic acid on amine-functionalized zirconia by exploitation of ionic interactions. The catalytic efficiency of the catalyst in the selective esterification of maleic acid with butan-1-ol to afford dibutyl maleate was investigated.

Results and Discussion

Physicochemical Characterization

Amine-functionalized zirconia (denoted as $AZrO_2$) was prepared by a sol-gel technique at basic pH with use of sodium hydroxide. Hydrolysis and condensation of zirconyl oxychloride ($ZrOCl_2$) and (3-aminopropyl)triethoxysilane (APTES) in the presence of ionic surfactant leads to the formation of mesoporous zirconia functionalized with amine groups. The surfactant-free amine-functionalized mesoporous zirconia was obtained by acid treatment of the as-synthesized zirconia. Silicotungstic acid was immobilized in the mesopores of amine-functionalized zirconia (denoted as SW-$AZrO_2$) by exploitation of simple ionic interaction as represented in Scheme 1. The amount of tungsten present in SW-$AZrO_2$ was found to be 34.7 %. Hence, 2.9 % of the silicotungstic acid had been immobilized in the pores of the zirconia.

The immobilization of silicotungstic acid and the nature of its interaction with amine-functionalized zirconia was confirmed by X-ray photoelectron spectroscopy and FTIR analysis. The wide scan of SW-$AZrO_2$ confirmed the presence of W, Si, Zr, N, C and O (Figure S1 in the Supporting Information).

The binding energy peaks (W $4f_{7/2}$, W $4d_{5/2}$ and W $4d_{3/2}$) observed at 36.00 eV (Figure 1, a), 248.28 eV (Figure 1, b) and 250.96 eV (Figure 1, b), respectively, were attributed to the +6 oxidation state of tungsten.[38–40] Figure 1 (c) shows the well resolved spin-orbit components for Zr $3d_{5/2}$ and Zr $3d_{3/2}$ peaks at 183.25 eV and 185.85 eV, respectively, which further confirmed the Zr^{4+} oxidation state.[33,41,42,43] The presence of two types of Si (Si–C and Si–O–W) was clearly evident from the deconvoluted spectra of Si 2p peaks (Figure 1, d). The peaks at 102.41 and 103.01 eV correspond to $2p_{3/2}$ and $2p_{1/2}$ of Si in the APTES moiety. Similarly, binding energies of $2p_{3/2}$ and $2p_{1/2}$ in the silicotungstate anion were observed at 103.42 and 104.42 eV, respectively.[44] The N 1s signal (Figure 1, e) showed three constituents at 400.55 eV, 402.17 eV and 402.83 eV, which corresponded to the presence of amino group, ammonium (NH_3^+) and NO species, respectively.[45] The presence of NH_3^+ confirmed the proton exchange between the silicotungstic acid and the free amine. The exact mechanism for the formation of NO species under alkaline conditions is not understood. The presence of free amine might be due to proton exchange between propylammonium and free surface hydroxy groups on zirconia. This exchange reaction can happen only under XPS conditions (high vacuum) through removal of water molecules. In a catalytic reaction this effect is negligible, due to the presence of solvent butan-1-ol around the active species. The presence of the propyl group in the silane moiety was observed in the narrow-scan spectra of C 1s (Figure S2). The aliphatic carbon atoms of C–C–H, C–N and C–C=O systems were observed at 285.05, 286.46 and 289.97 eV, respectively.[46] O1s XPS curve fitting[43] (Figure 1, f) showed peaks at 529.49 eV and 530.34 eV attributed to the presence of ZrO_2 and Si–O–Zr bonds, respectively. The peaks at 530.99 eV and 532.18 eV were due to the contributions of W–O–W and W–O–Si bonds, respectively. The peak at 533.34 eV was assigned to free OH groups present on the zirconia. The binding energy of carbonyl oxygen is observed at 531.49 eV. The formation of OH groups on the surface might be due to partial condensation of Zr–OH groups.

The successful immobilization was further confirmed by the FTIR spectrum, as shown in (Figure 2). $AZrO_2$ and SW-$AZrO_2$ each showed a broad peak at 3000 cm^{-1}, confirming the presence of adsorbed water molecules. Alkyl stretching vibrations of the aminopropyl groups were identified at 2950 cm^{-1} as a shoulder on the hydroxy broad peak, whereas amino group stretching vibrations were overlapped with the broad hydroxy peaks (not shown). CN stretching was observed at 1379 cm^{-1} in $AZrO_2$. The N–H bending vibration at 686 cm^{-1} and a shoulder at 1520 cm^{-1} assigned to the NH_2 symmetric bending vibration confirmed the presence of amine groups on the surfaces of the zirconia nanoparticles. The peaks at 712 cm^{-1} and 952 cm^{-1} corresponded to Zr–O bond and Zr–O–Si bonds.[30] The asymmetric stretching vibrations of tungsten–oxygen octahedra for pure silicotungstic acid (spectrum not shown) were

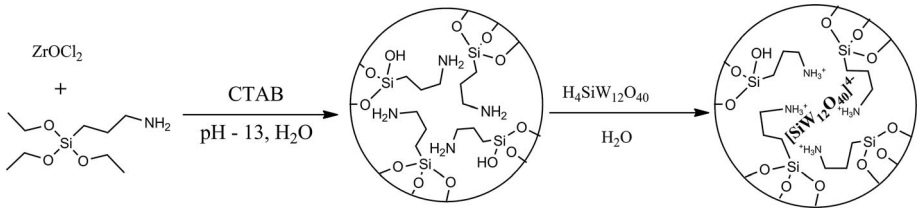

Scheme 1. Immobilization of silicotungstic acid on amine-functionalized mesoporous zirconia.

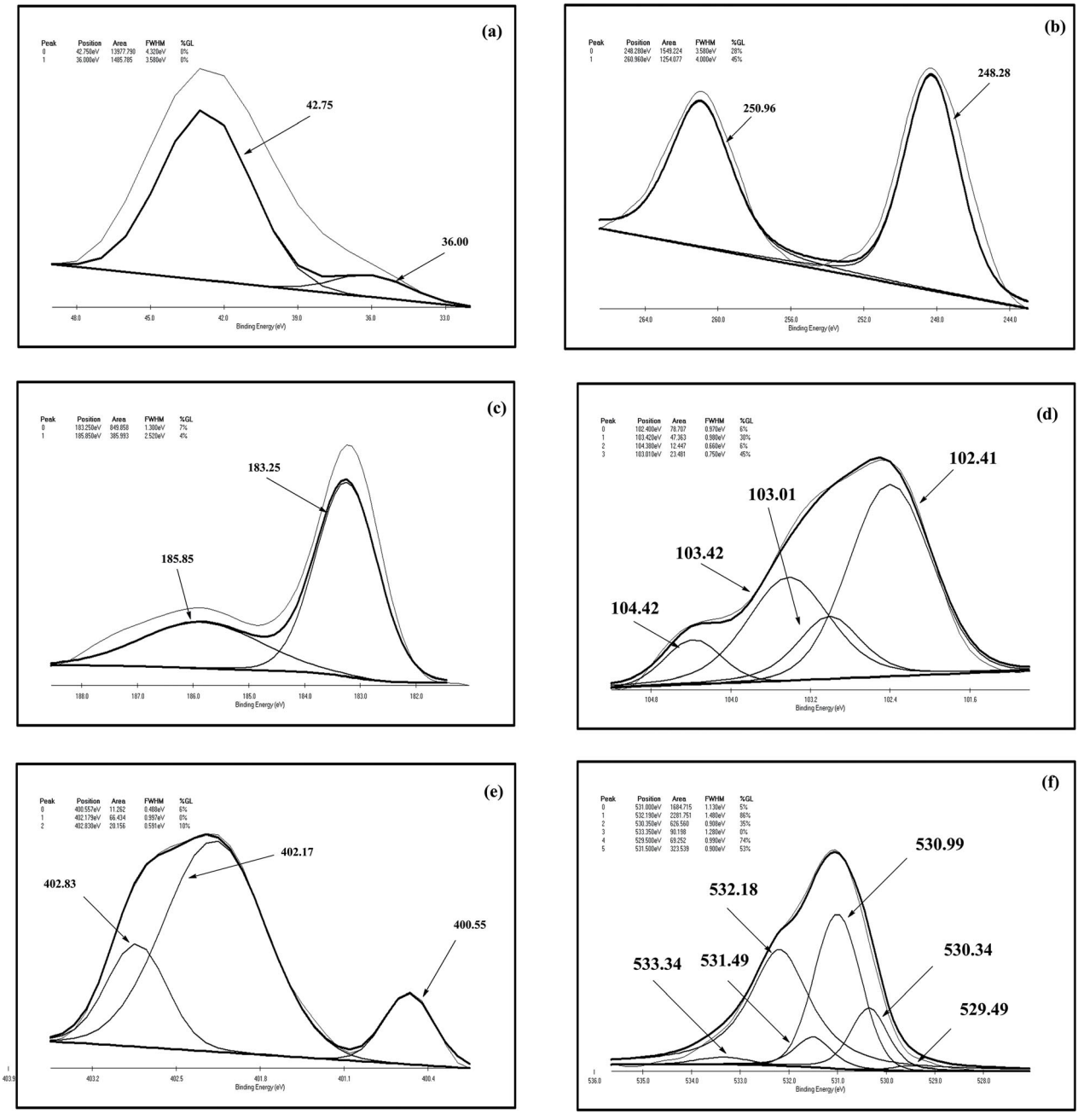

Figure 1. XPS depth profile spectra of SW-$AZrO_2$: (a) W 4f, (b) W 4d, (c) Zr 3d, (d) Si 2p, (e) N 1s, (f) O 1s. The spectra are normalized to aid visualization.

found as terminal (W–O_t), edge sharing (W–O_e–W) and corner sharing (W–O_c–W) peaks in the 981 cm^{-1}, 780 cm^{-1} and 880 cm^{-1} regions, respectively. The stretching mode of central SiO_4 tetrahedra was observed at 926 cm^{-1}.[14] The immobilization of silicotungstic acid in the pores of functionalized zirconia (SW-$AZrO_2$) was easily identified by the presence of stretching vibrations of WO_6 octahedra and SiO_4 tetrahedra. The peak at 912 cm^{-1} corresponds to the asymmetric stretching of Si–O. The prominent peak of tungsten octahedra, W–O_t, appeared as a shoulder at 1024 cm^{-1}, due to overlapping with the Zr–O–Si band. The other vibrations of tungsten octahedra, edge sharing (W–O_e–W) and corner sharing (W–O_c–W), were detected at 787 cm^{-1} and 871 cm^{-1}, respectively.

N_2 adsorption/desorption isotherms of $AZrO_2$ and SW-$AZrO_2$ are as shown in Figure 3 (a and b). Each sample corresponded to a type-IV isotherm, with a characteristic hysteresis loop confirming its mesoporous nature. The BET surface area for $AZrO_2$ was 52.56 $m^2\ g^{-1}$ whereas that for SW-$AZrO_2$ was 42.03 $m^2\ g^{-1}$. A considerable decrease in the BET surface area and pore volume as shown in Table 1 suggested that silicotungstic acid has been immobilized on the inner surface of the pores. The NLDFT method was used to calculate the pore size distribution of the $AZrO_2$ and SW-$AZrO_2$ samples. The inset in Figure 3 (a and b) shows the pore size distributions of the samples, with pore dimensions of 5.6 nm and 4.3 nm for $AZrO_2$ and SW-$AZrO_2$, respectively.

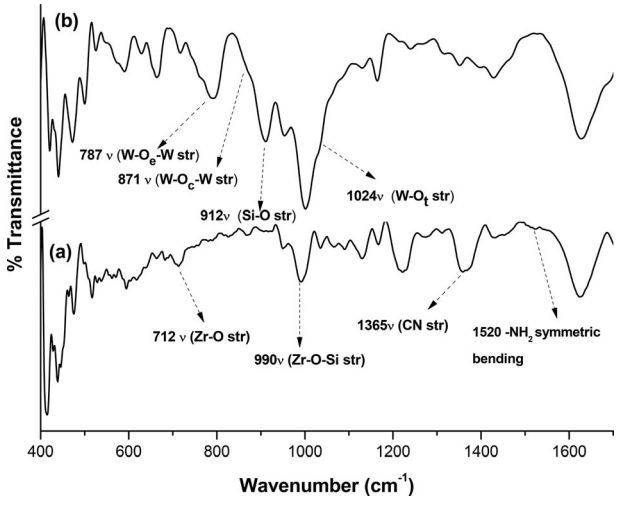

Figure 2. Combined FTIR spectrum of (a) $AZrO_2$, and (b) SW-$AZrO_2$.

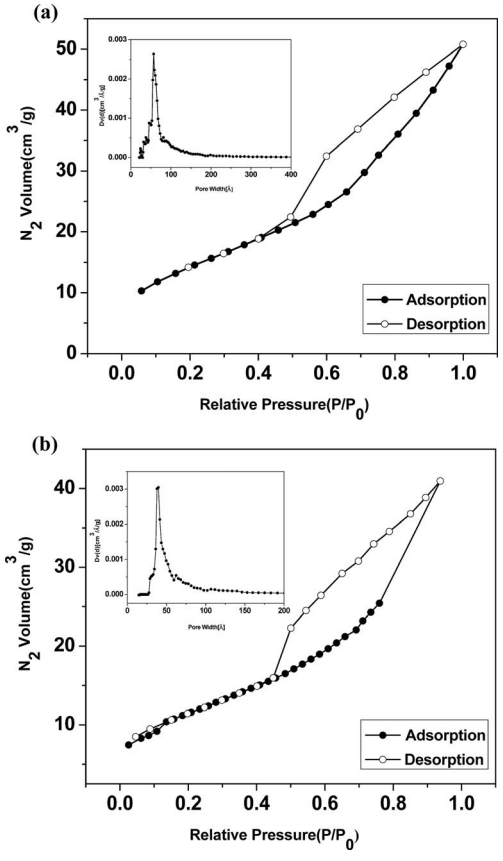

Figure 3. N_2 adsorption/desorption isotherms of (a) $AZrO_2$ (inset: pore size distribution graph), and (b) SW-$AZrO_2$ (inset: pore size distribution graph).

Table 1. Surface properties of silicotungstic acid immobilized on amine-functionalized mesoporous ZrO_2.

Sample name	Surface area [$m^2\ g^{-1}$]	Pore volume [cc g^{-1}])	Pore diameter [nm]
$AZrO_2$	52.56	0.0745	5.6
SW-$AZrO_2$	42.03	0.0611	4.3

Wide-angle X-ray diffraction patterns of $AZrO_2$ and SW-ZrO_2 are shown in Figure 4. In $AZrO_2$, no crystalline diffraction peaks were observed, as previously reported by Parida et al.[33] A similar pattern was observed for SW-ZrO_2, which indicated the amorphous nature of the catalyst. Moreover, the crystalline phases of silicotungstic acid were not observed, mainly due to the lower loading (2.9 %) and uniform dispersion of the active species. TEM images of SW-$AZrO_2$ (Figure 5) showed uniform spherical morphology. The EDX analysis confirmed the immobilization of silicotungstic acid in the pores of the amine-functionalized zirconia.

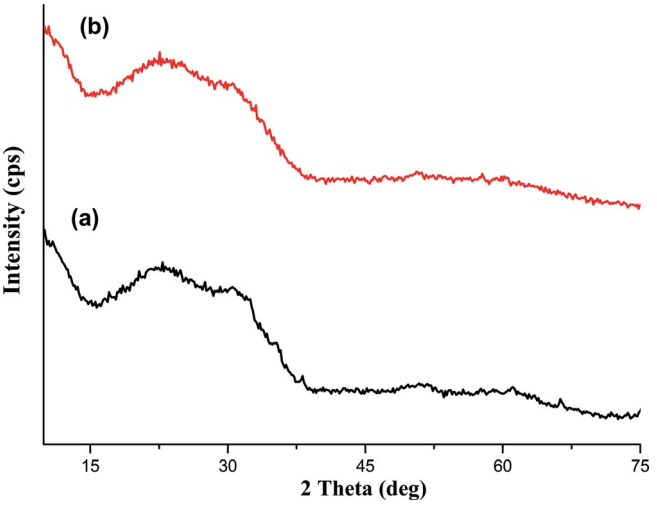

Figure 4. PXRD patterns of (a) $AZrO_2$, and (b) SW-$AZrO_2$.

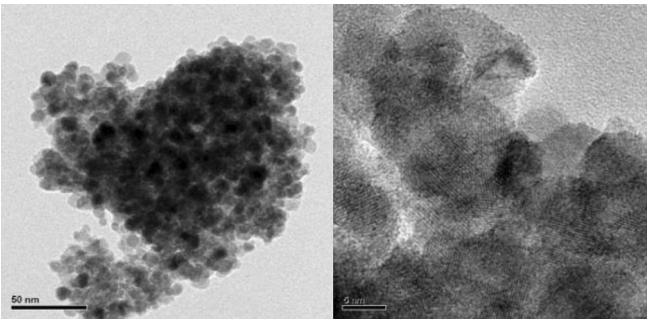

Figure 5. TEM images of SW-$AZrO_2$.

TGA patterns of the prepared samples under air are shown in Figure 6. $AZrO_2$ showed three distinct regions of weight loss (Figure 6, a).[33] The weight loss around 100 °C corresponds to the loss of water adsorbed on the sample. The weight loss observed between 150–250 °C was mainly due to the organic amine group grafted on the surface of the zirconia. The weight loss around 600 °C corresponds to the removal of terminal hydroxy groups bonded on to the surface of the zirconia. The TGA pattern of SW-$AZrO_2$ showed two distinct regions of weight loss (Figure 6, b). The weight loss observed in the 300–600 °C region corresponded to the decomposition of Keggin $[SiW_{12}O_{40}]^{4-}$ anion. The loss around 700 °C is attributed to the formation of defective WO_3^- anion.[14]

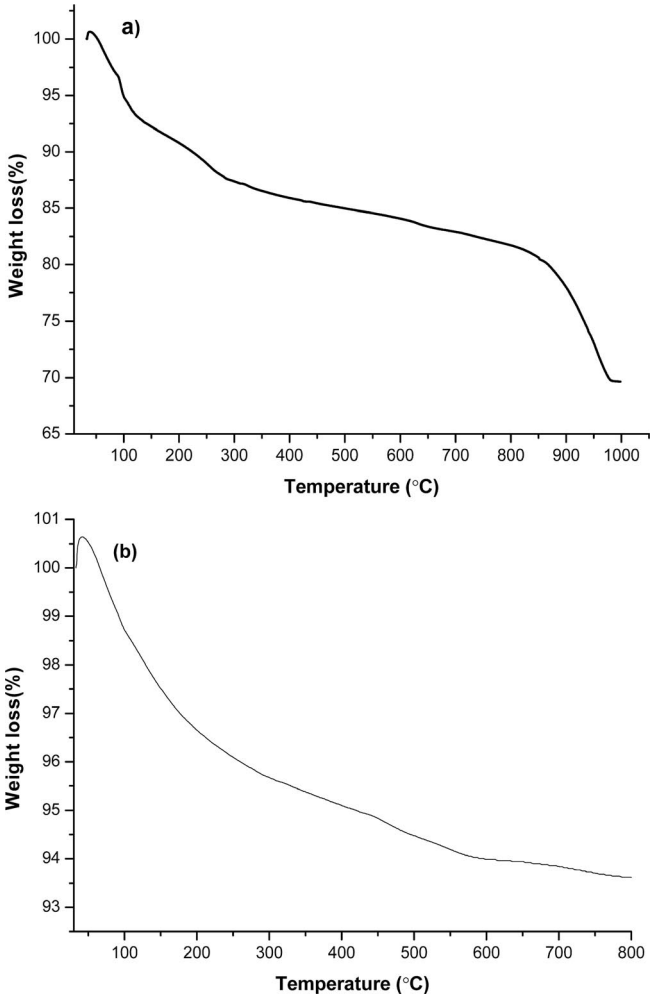

Figure 6. TGA patterns of (a) $AZrO_2$, and (b) SW-$AZrO_2$.

UV/Vis diffuse reflectance spectra of $AZrO_2$ showed two absorption bands at 215 and 293 nm due to charge transfer from oxo anion O^- to zirconium cation Zr^{4+} (Figure S3).[33] In the spectrum of SW-$AZrO_2$ the second of these peaks had shifted from 293 nm to 253 nm, indicating the electrostatic interaction and subsequent immobilization of Keggin anion $[SiW_{12}O_{40}]^{4-}$ to the pores of $AZrO_2$.

Catalytic Esterification

The catalytic activity of SW-$AZrO_2$ was evaluated for the liquid-phase esterification of maleic acid with butan-1-ol at 95 °C (Scheme 2). The products monobutyl maleate (MBM) and dibutyl maleate (DBM) were identified by GC–MS (Figures S4 and S5). The electrostatic interaction between silicotungstate anion and propylammonium cation, as evidenced from XPS analysis, generates a hydrophilic environment in the pores of the zirconia. This hydrophilic environment allows the easy diffusion of polar starting materials (maleic acid and butan-1-ol) into the pores and also allows easy separation of DBM (i.e., a hydrophobic product) as soon as it is formed. The reaction conditions, such as catalyst weight, butan-1-ol/maleic acid feed ratio and temperature, were varied to optimize the selectivity in favour of dibutyl maleate.

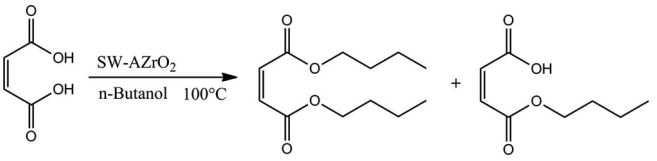

Scheme 2. Esterification of maleic acid catalysed by SW-$AZrO_2$.

To investigate the effect of catalyst concentration, the reaction was performed with an increase in the weight of catalyst present, from 50 to 150 mg. Initially, the selectivity was strongly in favour of MBM, but as the reaction proceeded the percentage decreased considerably, as shown in Figure 7. This is mainly because MBM is retained in the pores due to its amphiphilic nature and further reacts with butan-1-ol to give DBM. An increase in the weight of catalyst present increased the percentage selectivity with respect to DBM (Figure 8), and equilibrium was attained due to the simultaneous accumulation of water molecules in the hydrophilic sites of the catalyst. The formation of dibutyl fumarate was also observed, but always with <6 % selectivity. The degrees of conversion of maleic acid and the selectivity in favour of dibutyl maleate after 5 h were similar for 125 mg and 150 mg of catalyst. Hence, the optimum catalyst concentration was concluded to be 125 mg. High levels of conversion and selectivity in favour of dibutyl maleate were attained in shorter reaction times (i.e., 5 h) with SW-ZrO_2 as catalyst than with other solid acid catalysts, which exhibited similar results only after 9 h.[35,37]

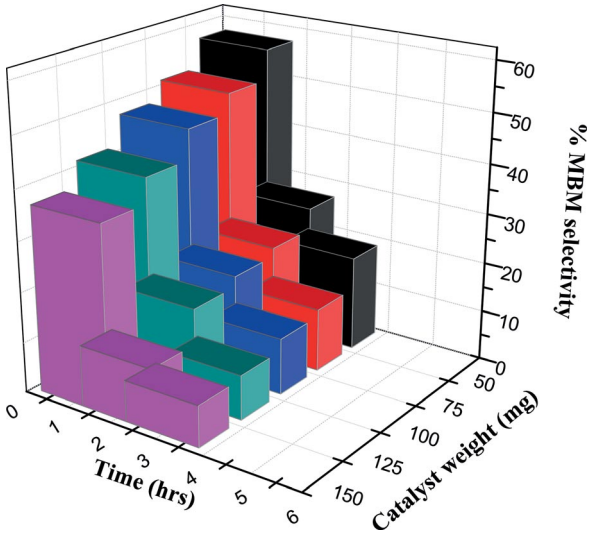

Figure 7. Effect of catalyst on MBM selectivity.

The feed ratio of butan-1-ol to maleic acid was varied from 10.95 mmol to 43.71 mmol. As expected, the level of conversion and the selectivity in favour of DBM decreased when the feed ratio of butan-1-ol to maleic acid was increased. The poorer accessibility of maleic acid to the hydrophilic sites is mainly due to the presence of excess butan-1-ol. The changes in the DBM product selectivity are as shown in Figure 9. A low feed ratio increased the selectivity in favour of DBM, but the reaction pro-

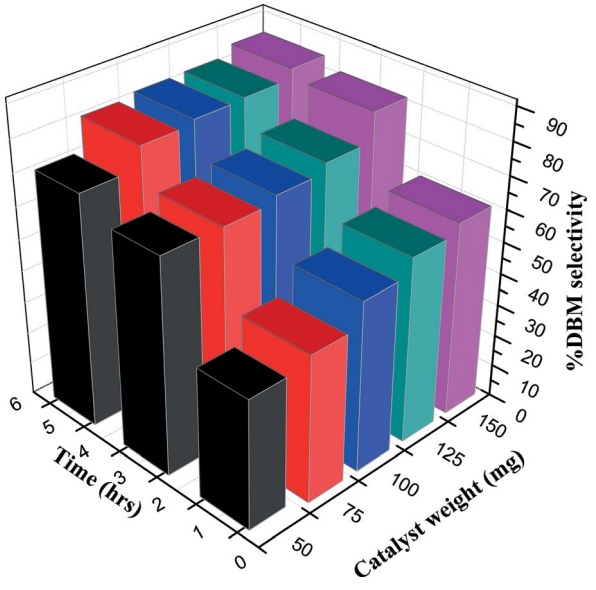

Figure 8. Effect of catalyst on DBM selectivity.

ceeded in a solvent-free manner rather than in a liquid-phase process. After 5 h, the attainment of maximum selectivity in favour of DBM was achieved when a feed ratio of 21.85 mmol was used, and hence this was concluded to be the optimum condition for the esterification.

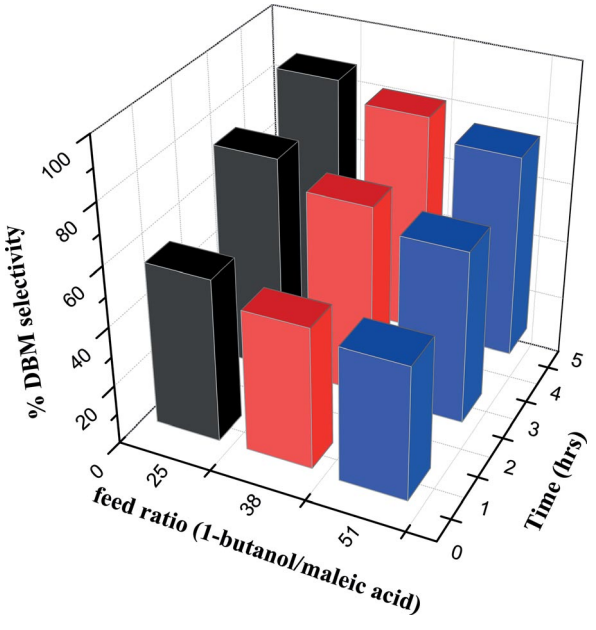

Figure 9. Effect of feed ratio on DBM selectivity.

The esterification was studied at three different temperatures: 85, 95 and 120 °C. High selectivity in favour of dibutyl maleate was observed with an increase in temperature (Figure 10). Although better conversion and selectivity were observed at 120 °C, the optimum temperature was chosen as 95 °C, because a higher temperature would result in leaching of the active species.

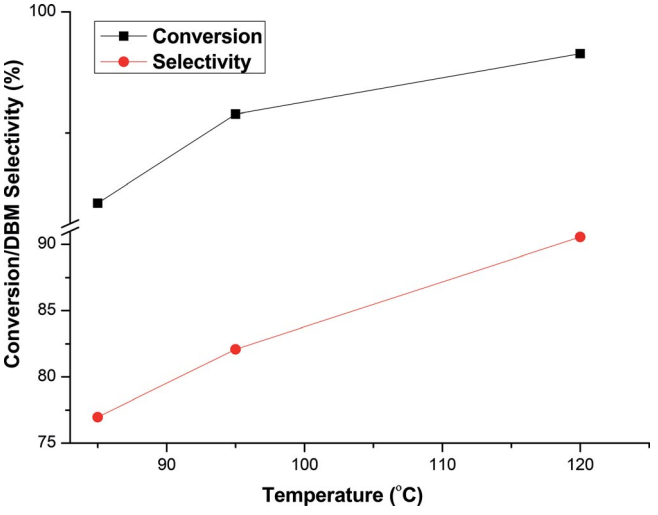

Figure 10. Effect of temperature on conversion and DBM selectivity.

DBM Selectivity

Under the optimum conditions, the effects of various forms of active species on maleic acid esterification were examined. The degrees of conversion and the selectivity in favour of DBM are tabulated in Table 2. Firstly, use of the active species of the catalyst (i.e., silicotungstic acid itself) resulted in >98 % conversion and >98 % selectivity in favour of dibutyl maleate with no isomerization. The better conversion and selectivity is achieved because silicotungstic acid possesses higher specific activity per unit proton than conventional acid catalysts. Complete catalyst recovery could not be achieved, due to the high solubility of silicotungstic acid in polar solvents. The exchange of protons with excess tetrabutylammonium ions resulted in tetrakis(tetrabutylammonium) silicotungstate catalyst. Use of this heterogeneous catalyst – $(TBA)_4SiW_{12}O_{40}$ with no acidic hydrogens – resulted in 79 % conversion with only 58 % selectivity in favour of dibutyl maleate. From Table 2 it can be seen that the presence of silicotungstic acid ($SW\text{-}AZrO_2$) had an immense effect on the selectivity in favour of DBM (i.e., 85 % with 98 % conversion, similar to the results obtained with pure silicotungstic acid). This indicates that the acid strength of the catalyst played an important role in the esterification reaction.[47] This catalyst, being heterogeneous in nature, was easily recovered by simple centrifugation.

Table 2. Esterification of maleic acid catalysed by different cation-substituted silicotungstates.[a]

Sl. No.	Catalyst	Conversion [%]	Selectivity [%]	
			DBM	DBF
1	$H_4SiW_{12}O_{40}$[b]	98.72	98.36	–
2	$(TBA)_4SiW_{12}O_{40}$	79.02	57.90	trace
3	$SW\text{-}AZrO_2$	98.06	82.09	5.7

[a] Maleic acid (0.861 mmol), butan-1-ol (21.85 mmol), catalyst (0.125 g), 95 °C, 5 h. [b] Homogeneous conditions, $H_4SiW_{12}O_{40}$ (0.01 equiv.).

In order to test the effectiveness of the catalyst, a reusability test was performed under optimum conditions at 95 °C. The $SW\text{-}AZrO_2$ could easily be recovered from the reaction mass by simple centrifugation and was washed several times with di-

ethyl ether, dried and reused for the subsequent catalytic cycles. The small decrease in the level of conversion, from 98 % in run 1 to 97 % in run 3, indicated that the hydrophilic environment in the mesoporous zirconia is well preserved (Figure 11). The selectivity in favour of DBM is also well retained (82 % to 78 %) after the third run, indicating the efficiency of the catalyst. After the third run, the decrease in selectivity in favour of DBM is attributed to the isomerization of dibutyl maleate to dibutyl fumarate in the presence of free amine groups within the zirconia, due to leaching of active species.[48] The leaching might be due to the better solubility of silicotungstate anion in polar solvents, as well as to the high reaction temperature (95 °C). FTIR of the reused catalyst showed characteristic vibrations of silicotungstic acid with a decrease in intensity (Figure 12).

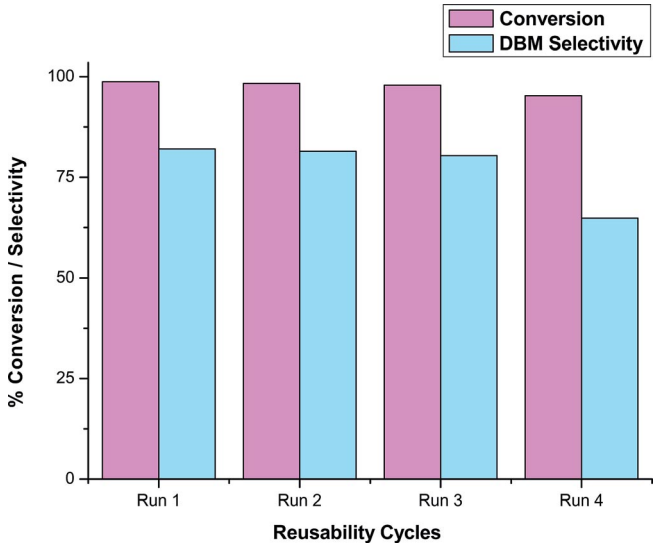

Figure 11. Reusability of SW-$AZrO_2$ in maleic acid esterification.

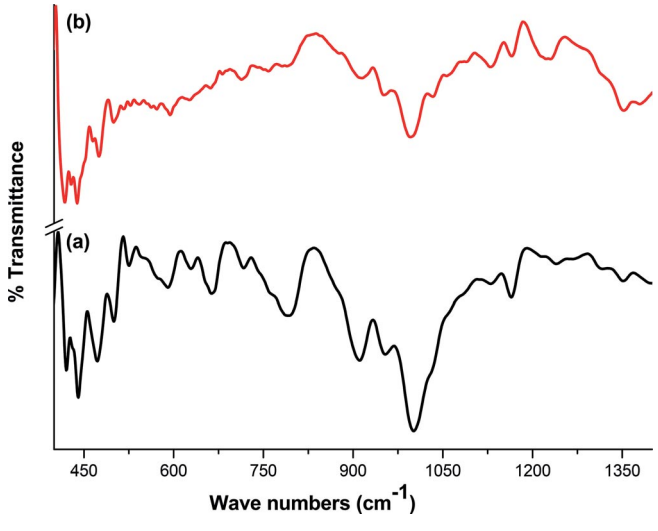

Figure 12. FTIR spectra of SW-ZrO_2: (a) fresh, (b) after fourth run.

Conclusions

In conclusion, the generation of a hydrophilic environment within the pores is achieved through simple electrostatic interaction between silicotungstic acid and amine-grafted zirconia. The presence of ammonium cations and silicotungstate anions within the mesopores was confirmed by FTIR, UV/Vis-DRS and XPS analysis. N_2 adsorption/desorption analysis confirmed the mesoporous nature of the samples. The decreases in surface area and pore volume clearly indicated the presence of silicotungstic acid within the pores of the amine-functionalized zirconia. This minimally loaded catalyst was found to be effective in selective esterification of maleic acid with 98 % conversion and better selectivity in favour of dibutyl maleate in a shorter reaction time (i.e., 5 h). Hence, this could be an eco-friendly alternative to the generally used hazardous mineral acids for the synthesis of dibutyl maleate.

Experimental Section

Materials: Zirconium oxychloride and APTES were purchased from Sigma–Aldrich. Cetyltrimethylammonium bromide (CTAB), sodium hydroxide, silicotungstic acid, maleic acid and butan-1-ol were purchased from Alfa Aesar and used as such without further purification.

Characterization: The W ion concentration determined by inductively coupled plasma–optical emission spectroscopy (ICP-OES, Perkin–Elmer OPTIMA 8000) was used to quantify the amount of tungsten content in SW-$AZrO_2$. The wavelength chosen was 207.91 nm and the limit of detection for tungsten was 7 ppb. The catalyst (100 mg), dispersed in sulfuric acid (10 M, 25 mL), was stirred at 85 °C for 24 h. This solution was diluted to the required volume and analysed for tungsten content by ICP-OES. X-ray photoelectron spectra were recorded with an ESCA-3 Mark II spectrometer (VG Scientific Ltd., UK) with Al-K_α (1486.6 eV) radiation as the source. Spectra were referenced to the binding energy of C1s (285 eV). The IR spectra of the samples were recorded in the ATR mode with a Jasco FT/IR-6300 instrument in the 4000–400 cm^{-1} range. The BET surface areas and pore size distributions of the materials were determined by N_2 adsorption measurements carried out with a Belsorp 28SA at 77 K. Prior to analysis, the samples were degassed at 150 °C for 3 h. The natures of the samples were analysed with high-angle X-ray diffractometers (Bruker A8) and use of Cu-K_α in the 2θ range of 10° to 90°. Transmission electron microscopy (TEM) was performed with a JEOL model JEM-2100 electron microscope equipped with an energy-dispersive X-ray spectroscopy (EDS) detector and operated at an accelerating voltage of 200 kV. The thermal stability was recorded with a Metler–Toledo Thermogravimetric Analyzer under oxygen (flow rate 20 mL min^{-1}) in the temperature range of 30–1000 °C at a heating rate of 5 °C min^{-1}. UV/Vis diffuse reflectance spectra (UV-DRS) were recorded with a Shimadzu UV 2401PC spectrophotometer and use of an integrating sphere attachment.[49–51] $BaSO_4$ was used as background standard.

Synthesis of Amine-Functionalized Mesoporous Zirconia ($AZrO_2$): Amine-functionalized zirconia was synthesized as reported by Parida et al.,[33] but with use of zirconium oxychloride instead of zirconium butoxide. A mixture of cetyltrimethylammonium bromide (0.025 mol, 2.8 g), sodium hydroxide (0.03 mol, 4 g) and water (4 mol, 72 mL) was heated at 80 °C for 30 min at a pH of 13. The zirconium oxychloride dissolved in water, APTES was added rapidly, and the mixture was stirred for 2 h. The resulting precipitate was filtered, washed with water followed by methanol and dried under vacuum. The surfactant was removed by acid extraction, with the

material (1 g) being treated with a mixture of ethanol (100 mL) and conc. HCl (1 mL, 38 % in weight) at 80 °C for 6 h. The resulting product was filtered, washed with ethanol and dried.

Synthesis of Silicotungstic Acid Supported on Amine-Functionalized Mesoporous Zirconia (SW-AZrO$_2$): Silicotungstic acid ($H_4[SiW_{12}O_{40}]$, 0.3 g) was added to $AZrO_2$ (1 g) dispersed in water (20 mL), and the mixture was stirred at 60 °C for 24 h. The obtained precipitate was filtered off, washed with excess water to remove unreacted silicotungstic acid and dried under vacuum for 6 h. The synthesis of the catalyst is shown in Scheme 1. Tetrakis(tetrabutylammonium) silicotungstate was prepared by the same procedure with tetrabutylammonium bromide instead of 1-butyl-3-methylimidazolium bromide.[14]

Catalytic Procedure for Esterification of Maleic Acid with Butan-1-ol: Esterification of maleic acid with butan-1-ol was carried out in a two-necked round-bottomed flask at 95 °C for 5 h. Maleic acid (0.861 mmol) was added to a stirred dispersion of catalyst (125 mg) in butan-1-ol (2 mL). Small aliquots of sample were withdrawn periodically (1, 3 and 5 h) and monitored for the progress of the reaction by gas chromatography (Shimadzu 2014) with use of a capillary column (Rtx-5, 30 m × 0.32 mm ID × 1 μm) and FID detector. Nitrogen was used as the carrier gas at a flow rate of 37.1 mL min^{-1} and a column flow of 1.1 mL min^{-1}. The products were confirmed by GC–MS (Perkin–Elmer). A Clarus 680 chromatograph with capillary column (Elite-5MS, 30 m × 0.25 mm ID × 250 μm df) was connected to a Clarus 600 (EI) mass spectrometer. The maleic acid conversion and product selectivity was calculated by use of the equation given below.

$$\text{Conversion (mol-\%)} = \frac{\text{Initial mol-\% – Final mol-\%}}{\text{Initial mol-\%}} \times 100$$

$$\text{Selectivity in favour of dibutyl maleate (\%)} = \frac{\text{GC peak area of dibutyl maleate}}{\text{Sum of GC peak area of monobutyl and dibutyl maleate}} \times 100$$

Supporting Information (see footnote on the first page of this article): Wide-scan XPS of SW-AZrO$_2$, C 1s narrow scan of SW-AZrO$_2$, UV/Vis diffuse reflectance spectra of $AZrO_2$ and SW-AZrO$_2$, mass spectrum of monobutyl maleate, mass spectrum of dibutyl maleate.

Acknowledgments

We would like to thank the following organizations for lab space, supplies and equipment. The authors thank the Department of Science and Technology (DST), New Delhi (grant number SR/S3/CE/23/2008), the Department of Chemical Engineering IIT-Madras, the Directorate of Extramural Research & Intellectual Property Rights, Defence Research and Development Organization (ER&IPR, DRDO) (grant number ERIP/ER/0800344/M/01/1098), and the Council of Industrial and Scientific Research (CSIR), New Delhi (grant number 01 (2226)/08/EMR-II) for financial support. B. S. Abdur Rahman University is duly acknowledged for characterization of samples (FTIR and GC). The Amrita Centre for Nanosciences and Molecular Medicine, Kochi, is gratefully acknowledged for XPS analysis. The authors are grateful to the PSG Institute of Advanced Studies, Coimbatore, for TEM characterization and thank Startech Labs PVT Ltd., Hyderabad, for offering ICP-OES support.

Keywords: Silicotungstic acid · Mesoporous materials · Zirconia · Polyoxometallates · Electrostatic interactions · Supported catalysts

[1] I. V. Kozhevnikov, *Chem. Rev.* **1998**, *98*, 1–390. The entire issue is devoted to polyoxometallates.
[2] T. Okuhara, N. Mizuno, M. Misono, *Adv. Catal.* **1996**, *41*, 113–252.
[3] C. L. Hill, C. Chrisina, M. Prosser-McCartha, *Coord. Chem. Rev.* **1995**, *143*, 407–455.
[4] N. Mizuno, K. Yamaguchi, K. Kamata, *Coord. Chem. Rev.* **2005**, *249*, 1944–1956.
[5] G. Yihang, H. Changwen, *J. Mol. Catal. A* **2007**, *262*, 136–148.
[6] F. Saeid, B. Zaynab, M. Mansoureh, *Acta Chim. Solv.* **2006**, *53*, 72–76.
[7] Y. Hongxun, L. Tianfu, C. Minna, L. Hongfang, G. Shuiying, C. Rong, *Chem. Commun.* **2010**, *46*, 2429–2431.
[8] K. Jun, N. Yoshinao, U. Sayaka, Y. Kazuya, M. Noritaka, *Chem. Eur. J.* **2006**, *12*, 4176–4184.
[9] Y. Kazuya, Y. Chie, U. Sayaka, M. Noritaka, *J. Am. Chem. Soc.* **2005**, *127*, 530–531.
[10] L. Xianjun, L. Zhen, X. Chungu, *Synth. Commun.* **2008**, *38*, 1610–1616.
[11] Y. Shi Xian, F. Wei Jun, *J. Mol. Catal. A* **2008**, *280*, 142–147.
[12] M. D. Tzirakis, I. N. Lykakis, M. Orfanopoulos, *Chem. Soc. Rev.* **2009**, *38*, 2609–2621.
[13] B. Ankur, F. Lefebvre, S. B. Halligudi, *J. Catal.* **2007**, *247*, 166–175.
[14] a) T. Rajkumar, G. Ranga Rao, *Mater. Chem. Phys.* **2008**, *112*, 853–857; b) R. Thouvenot, M. Fournier, R. Franck, C. Rocchiccioli-Deltcheff, *Inorg. Chem.* **1984**, *23*, 598–605.
[15] T. Rajkumar, G. Ranga Rao, *Mater. Lett.* **2008**, *62*, 4134–4136.
[16] L. Baoshan, M. Wei, L. Jianjun, Z. Shengli, L. Xianfen, *J. Colloid Interface Sci.* **2011**, *362*, 42–49.
[17] M. Biju Devassy, S. B. Halligudi, *J. Catal.* **2005**, *236*, 313–323.
[18] B. Siddhartha Kumar, D. Dipak Kumar, *Appl. Clay Sci.* **2011**, *53*, 347–352.
[19] J. H. Sepúlveda, J. C. Yori, C. R. Vera, *Appl. Catal. A* **2005**, *288*, 18–24.
[20] a) F. Bentaleb, O. Makrygenni, D. Brouri, C. Coelho Diogo, A. Mehdi, A. Proust, F. Launay, R. Villanneau, *Inorg. Chem.* **2015**, *54*, 7607–7616; b) L. Xiujuan, Y. Chun, *PhysChemChemPhys* **2011**, *13*, 7892–7902.
[21] a) T. Aliakbar, A. Mansour, N. Ali, K. Maryam, M. A. Mostafa, *J. Colloid Interface Sci.* **2006**, *303*, 32–38; b) I. Kei, I. Toru, K. Yuichi, O. Toshio, Y. Shoji, *Angew. Chem. Int. Ed.* **2007**, *46*, 7625–7628; *Angew. Chem.* **2007**, *119*, 7769.
[22] F. Hoffmann, M. Cornelis, J. Morell, M. Fröba, *Angew. Chem. Int. Ed.* **2006**, *45*, 3216–3251; *Angew. Chem.* **2006**, *118*, 3290.
[23] R. Gopalan, C. H. Chang, Y. S. Lin, *J. Mater. Sci.* **1995**, *30*, 3075–3081.
[24] M. Yuichi, K. Shin-ichi, K. Katsuya, *J. Asian Cer. Soc.* **2014**, *2*, 11–19.
[25] S. Euaggelia, N. L. Ioannis, S. A. Gerasimos, *RSC Adv.* **2014**, *4*, 8402–8409.
[26] G. S. Armatas, G. Bilis, M. Louloudi, *J. Mater. Chem.* **2011**, *21*, 2997–3005.
[27] K. M. Parida, M. Sujata, *J. Mol. Catal. A* **2007**, *275*, 77–83.
[28] S. Zhou, G. Garnweitner, M. Niederberger, M. Antonietti, *Langmuir* **2007**, *23*, 9178–9187.
[29] S. Scholz, S. Kaskel, *J. Colloid Interface Sci.* **2008**, *323*, 84–91.
[30] A. Tarafdar, P. Pramanik, *Microporous Mesoporous Mater.* **2006**, *91*, 221–224.
[31] K. Luo, S. Zhou, L. Wu, G. Gu, *Langmuir* **2008**, *24*, 11497–11505.
[32] K. M. Parida, S. Mallick, P. C. Sahoo, S. K. Rana, *Appl. Catal. A* **2010**, *381*, 226–232.
[33] M. Sujata, R. Surjyakanta, K. Parida, *Dalton Trans.* **2011**, *40*, 9169–9175.
[34] A. Zaidi, J. L. Gainer, G. Carta, *Biotechnol. Bioeng.* **1995**, *48*, 601–605.
[35] M. Bhagiyalakshmi, K. Shanmugapriya, M. Palanichamy, A. Banumathi, V. Murugesan, *Appl. Catal. A* **2004**, *267*, 77–86.
[36] B. Makowka, H. Block, Bayer Aktiengesellschaft, US Patent 4827022, **1989**.
[37] M. Bhagiyalakshmi, S. Vishnu Priya, J. Herbert Mabel, M. Palanichamy, V. Murugesan, *Catal. Commun.* **2008**, *9*, 2007–2012.
[38] K. T. Venkateswara Rao, P. S. Sai Prasad, N. Lingaiah, *Green Chem.* **2012**, *14*, 1507–1514.
[39] F. J. Berry, G. R. Derrick, J. F. Marco, M. Mortimer, *Mater. Chem. Phys.* **2009**, *114*, 1000–1003.

[40] A. Romanyuk, R. Steiner, L. Marot, P. Oelhafen, *Sol. Energy Mater. Sol. Cells* **2007**, *91*, 1831–1835.
[41] Y. Suchorski, R. Wrobel, S. Beckerb, A. Opalinska, U. Narkiewicz, M. Podsiadly, H. Weiss, *Acta Phys. Pol. A* **2008**, *114*, S125–134.
[42] D. D. Sarma, C. N. R. Rao, *J. Electron Spectrosc. Relat. Phenom.* **1980**, *20*, 25–45.
[43] C. Y. K. Lung, M. G. Botelho, M. Heinonen, J. P. Matinlinna, *Dental Mater.* **2012**, *28*, 863–872.
[44] A. Thogersen, J. H. Selj, E. S. Marstein, *J. Electrochem. Soc.* **2012**, *159*, D276–D281.
[45] H. J. Martin, K. H. Schulz, J. D. Bumgardner, K. B. Walters, *Langmuir* **2007**, *23*, 6645–6651.
[46] a) B. K. Sodipo, A. A. Aziz, *Beilstein J. Nanotechnol.* **2014**, *5*, 1472–1476; b) R. G. Acres, A. V. Ellis, J. Alvino, C. E. Lenahan, D. A. Khodakov, G. F. Metha, G. G. Andersson, *J. Phys. Chem. C* **2012**, *116*, 6289–6297.
[47] H. Liu, N. Xue, L. Peng, X. Guo, W. Ding, Y. Chen, *Catal. Commun.* **2009**, *10*, 1734–1737.
[48] K. Nozaki, *J. Am. Chem. Soc.* **1941**, *63*, 2681–2683.
[49] S. K. Das, M. K. Bhunia, A. Bhaumik, *Dalton Trans.* **2010**, *39*, 4382–4390.
[50] A. Modak, J. Mondal, M. Sasidharan, A. Bhaumik, *Green Chem.* **2011**, *13*, 1317–1331.
[51] S. Dutta, A. Patra, S. De, A. Bhaumik, B. Saha, *ACS Appl. Mater. Interfaces* **2012**, *4*, 1560–1564.

Received: December 6, 2015
Published Online: March 17, 2016

